Received: 4 November 2016 | Revised: 22 July 2017 | Accepted: 13 December 2017
DOI: 10.1002/we.2168

RESEARCH ARTICLE

WILEY

Validation of a hybrid modeling approach to floating wind turbine basin testing

Matthew Hall[1] | Andrew J. Goupee[2]

[1]School of Sustainable Design Engineering, University of Prince Edward Island, Charlottetown, PE C1A 4P3, Canada
[2]Department of Mechanical Engineering, University of Maine, Orono, Maine 04469, USA

Correspondence
Matthew Hall, School of Sustainable Design Engineering, University of Prince Edward Island, Charlottetown, PE C1A 4P3, Canada.
Email: mthall@upei.ca

Abstract

Hybrid modeling combining physical tests and numerical simulations in real time opens new opportunities in floating wind turbine research. Wave basin testing is an important validation step for floating support structure design, but current methods are limited by scaling problems in the aerodynamic loadings. Applying wind turbine loads with an actuation system controlled by a simulation that responds to the basin test offers a way to avoid scaling problems and reduce cost barriers for floating wind turbine design validation in realistic coupled conditions. In this work, a cable-based hybrid coupling approach is developed and implemented for 1:50-scale wave basin tests with the DeepCwind semisubmersible floating wind turbine. Tests are run with thrust loads provided by a numerical wind turbine model. Matching tests are run with physical wind loads using an above-basin wind maker. When the numerical submodel is set to match the aerodynamic performance of the physical scaled wind turbine, the results show good agreement with purely physical wind-wave tests, validating the hybrid model approach. Further hybrid model tests with simulated true-to-scale dynamic thrust loads and wind turbulence show noticeable differences and demonstrate the value of a hybrid model approach for improving the true-to-scale realism of floating wind turbine basin tests.

KEYWORDS

basin test, floating, hybrid model, hybrid testing, wind turbine

1 | INTRODUCTION

Scale-model testing of floating wind turbines, often considered an essential validation step in the design process, faces a difficult scaling problem. Two different fluid-structure-interaction domains need to be scaled simultaneously: the hydrodynamics of the floating support structure and the aerodynamics of the wind turbine. The dominance of different nondimensional ratios in each makes scaling without compensation cause discrepancies in the results. For example, a scaled-down floating wind turbine may require higher wind speeds and blade pitch adjustments to achieve the correct thrust force.[1] On top of this, there is the challenge of recreating a wind turbine's mechanical properties at small scale. For less advanced facilities, even providing controlled wind conditions above the wave basin may not be feasible. All these factors contribute to the scaling difficulty in floating wind turbine experiments.

A number of approaches have arisen in recent years to counter some of these challenges, especially to do with the turbine aerodynamics. Müller et al review many of the challenges and options for floating wind turbine basin testing.[2] The most direct approach is to compensate for performance reductions through changes to the rotor geometry. Martin et al explored enlarging the blades, using special airfoils, and adding leading edge roughness to counter the lowered Reynolds number.[3] Research at the University of Maine and the Maritime Research Institute of the Netherlands (MARIN) showed that using low-Reynolds number airfoils with enlarged chord lengths can come close to matching true-to-scale thrust coefficients across typical operating conditions.[4,5] However, this work has not yet shown the ability to also match torque characteristics, meaning that the scalability for details such as blade pitch control and its effect on aerodynamic damping is limited.

An alternative approach involves what can be called hybrid modeling: a real-time coupling of physical and numerical models. In this, the wind turbine aerodynamics are modeled numerically rather than physically, and this simulation is dynamically coupled with the remaining floating structure

experiment. A motion tracking system transmits physical platform motions to the wind turbine simulation, and an actuation system applies the calculated aerodynamic forces onto the floating platform experiment.[6-8]

The benefit of the hybrid approach comes from the versatility possible in simulations. Any scale can be modeled, avoiding the problem of low Reynolds number aerodynamics. Wind conditions can be specified with greater fidelity than may be possible physically. Blade-pitch control can be modeled without the limitations of small-scale actuation. Different turbine characteristics can even be explored at the push of a button. Furthermore, a hybrid approach avoids the need for above-basin wind generation, the equipment for which is only available at select facilities. This makes floating wind turbine basin testing more accessible to researchers.

Possible disadvantages of the hybrid approach should also be recognized. The results become subject to the quality of a numerical wind turbine model. Blade element momentum theory, the common modeling approach for medium fidelity simulation and use in hybrid models, relies on a number of assumptions and is known to lose accuracy when turbine motions are very large.[9-11] The quality of the coupling is another source of inaccuracies—whether from response limitations[7] or neglected degrees of freedom (DOFs) in the actuation.[12]

Simulation tools suitable for use in such a hybrid model, such as the FAST simulator developed by the National Renewable Energy Laboratory (NREL),[13] are readily available and can be adapted for hybrid coupling without great difficulty. Similarly, the physical portion of the model, a moored floating platform in a wave basin, is a relatively straightforward test. The main challenge is in creating the mechatronic system that couples the physical and numerical submodels together. One approach is described by Azcona et al[8] and uses a ducted fan mounted at the tower top to provide the wind turbine thrust force. Although the ducted fan had a limited ramping rate, Azcona et al showed that it gave good results in 1:40-scale tests when compared with simulations. Another approach, described by Chabaud,[14] is to use a system of winches connected around the tower top to apply the wind turbine thrust force and also, depending on arrangement, in-plane forces and moments. Bachynski et al demonstrated such an approach in 1:30-scale wave basin tests and produced realistic coupled response of the hybrid model including details such as blade-pitch control.[15,16]

While the cited literature describes 2 recent approaches that have been successfully used for hybrid model basin tests, a fully experimental validation of the approaches has not been given since this would require accompanying physical tests with above-basin wind generation. To fill that gap, the present study uses a combined wind and wave testing facility to conduct hybrid model tests alongside fully physical wind-wave tests, allowing experimental validation of the hybrid model approach.

The remainder of this paper is organized as follows. Section 2 describes a hybrid model coupling approach using an arrangement of 2 opposing cables attached to the turbine at hub height. The experimental and numerical realization of this approach is described in Section 3. In Section 4, physical and hybrid model test results are compared to validate the hybrid approach. Further tests use the hybrid model to simulate phenomena that are difficult to reproduce physically, demonstrating the new capabilities that can be realized. Conclusions about the validation and further opportunities offered by hybrid modeling are discussed in Section 5.

2 | HYBRID MODEL COUPLING APPROACH AND CONTROL FORMULATION

The tests presented in this paper use a cable-based approach to actuate wind turbine thrust forces on a floating platform as it moves. This approach is versatile and allows relatively fast response. Cables can cover a large workspace with very little mass that moves with the platform. Also, because each cable only constrains in a single direction, it is possible to apply forces along 1 axis while leaving the other degrees of freedom essentially unconstrained.

The so-called cable-driven parallel manipulators (CDPMs) have been studied since the 1990s as more versatile, affordable, and responsive alternatives to parallel manipulators with rigid links. Their low inertia allows for extremely high accelerations; 43 g accelerations and 13 m/s speeds were demonstrated with inexpensive 60 W motors[17] as early as 1995. This level of performance requires high cable tensions, achieved by making the cable system "redundant"—having at least one more cable than the number of platform DOFs being controlled. This allows the forces on the platform and the overall amount of tension in the cables to be controlled independently, ensuring that the cables maintain adequate tension at all times.[17,18] With different numbers and arrangements of winch units, any number of the 6 rigid-body DOFs can be controlled,[19] giving flexibility in which forces are applied on the floating platform.

The tests in this work use a system of 2 cables, pulling fore and aft on the nacelle, to actuate the wind turbine thrust force in the longitudinal direction on the physical model. The effect of aerodynamics on both surge and pitch is approximated by having the cable attachment at hub height. While this approach is thought to have minimal unwanted side effects on platform motions, it does neglect other aerodynamic force and moment components, as well as the gyroscopic effects of the rotor. Bachynski et al discuss the effects of actuation in limited DOFs.[12]

2.1 | Cable robot mechanics and control

The theory for describing the mechanics of CDPMs is well established (eg, Alp and Agrawal,[20] Roberts et al,[21] and Pott et al[22]). The present work makes the simplifying assumption of actuation in a single DOF. This follows directly from the more general multi-DOF formulation, which is developed in Hall. [23]

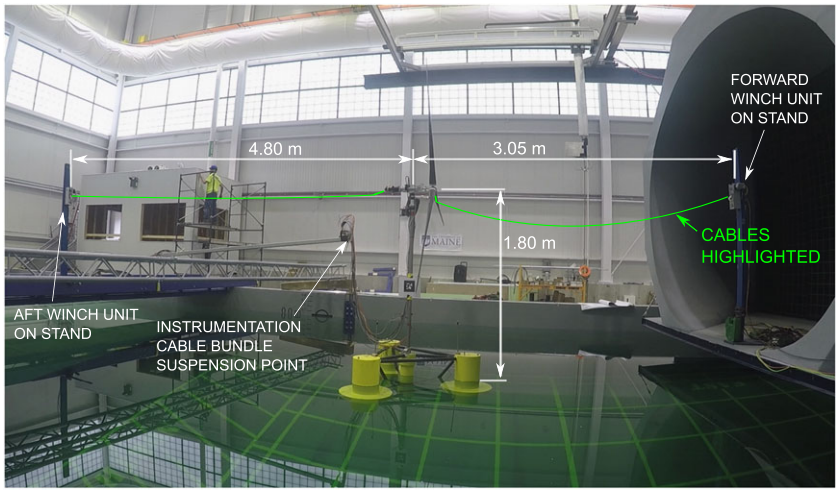

FIGURE 1 Arrangement of cable system in basin [Colour figure can be viewed at wileyonlinelibrary.com]

The test setup, with winches positioned to pull in opposite directions on the turbine nacelle (the coupling point of the hybrid model), is shown in Figure 1. Setting the spacing of the winch units to be much larger than the coupling point displacements allows the control problem to be approximated as 1-dimensional based on the fore-aft motions of the nacelle.

If x represents the coupling point translation in the downwind direction, and Δl_i represents the change in length of cable i (where $i = 1$ for downwind and $i = 2$ for upwind), then the requirement for maintaining constant cable tension is $\Delta l_1 = -x$ and $\Delta l_2 = x$. Using the Jacobian or structure matrix of the CDPM (see, eg, Pott et al[22]), the velocity and force relationships are equally simple. These equations are only approximate when tensions are not constant; however, small deviations can be compensated for through feedback control as described in the next section.

Key to CDPM control is the separation of overall cable tensions from the applied force.[19] This means that the necessary cable tension can be represented as a summation of 2 components: the desired mean cable tension, f_m, and the applied thrust force, w. For single-DOF actuation, the cable tensions in the downwind and upwind cables are, respectively,

$$\begin{aligned} f_1 &= f_m + w/2, \\ f_2 &= f_m - w/2. \end{aligned} \tag{1}$$

2.2 | Control

Control of the hybrid coupling system brings together 2 considerations: the mathematical rules defining the coupling between numerical and physical models and the means of ensuring that the forces or motions in the actuator are as desired. For defining the coupling in terms of a relationship between the kinematics and forces at the coupling point, the impedance control approach is well established in the robotics literature.[24] It uses measured physical motions as inputs to the numerical model and applies the calculated forces back onto the physical system. For a single DOF, this takes the form

$$w_d = F_{sim}(x, \dot{x}, \ddot{x}, t), \tag{2}$$

where w_d is the desired thrust force to be applied onto the physical system.

The impedance control scheme developed in this work uses 2 measurement types: optical sensing of the floating platform motions and load cell measurement of the cable tensions. The controller can be divided into 3 components, which are discussed in the following subsections.

2.2.1 | Tension feedback

The first control component is a proportional feedback loop that adjusts the cable length rate of change, $\dot{l}_{fi}$, based on measured tension, f_i:

$$\dot{l}_{fi} = -K_p(f_{di} - f_i), \tag{3}$$

where f_{di} is the desired cable tension according to (1) and K_p is the proportional gain. This feedback controller acts to maintain mean cable tensions and provides a limited ability to apply forces and compensate for motion. Figure 2 shows the control block diagram for the downwind cable ($i = 1$), assuming that the servomotor response time is negligible compared to that of the overall controller.

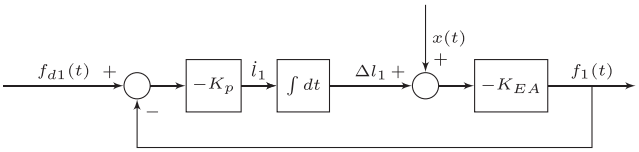

FIGURE 2 Tension control block diagram

Neglecting coupling point motion, x, the closed-loop response in the Laplace domain is

$$\frac{F(s)}{F_d(s)} = \frac{1}{\frac{s}{K_p K_{EA}} + 1}, \tag{4}$$

where $F(s)$ is the Laplace transform of $f(t)$. The controller bandwidth is $\omega_c = K_p K_{EA}$. If the coupling point moves, its velocity, $\dot{x}$, acts as a disturbance to the tension controller. The resulting tension response is

$$\frac{F(s)}{\dot{X}(s)} = \frac{K_{EA}}{s + K_{EA} K_p} = \frac{1}{K_p} \frac{1}{\frac{s}{K_p K_{EA}} + 1}. \tag{5}$$

This response is the same as (4) except that it is also scaled by $1/K_p$, revealing an important point. Subject to stability limits, disturbance rejection can be improved without affecting the tension-control bandwidth as long as the ratio K_{EA}/K_p is kept constant.

2.2.2 | Motion accommodation

Because the feedback controller has limited ability to reject motion disturbances, a second control component is used to proactively adjust cable lengths in response to measured coupling point motions. This requires a motion observer to calculate positions, velocities, and accelerations from the optical position measurements. These observed motions also serve as the inputs to the numerical submodel. Minimizing noise and latency is crucial for this purpose. For example, in a situation where a stiffness term in the numerical model acts to provide a restoring force on the physical model, any delay in the coupling can phase-shift the stiffness reaction such that negative damping is created.

The observer must be designed carefully since time-varying phase lags, such as can occur with a Kalman filter,[25] can make delay compensation difficult. Conversely, simple nth-order polynomial approaches to delay compensation (eg, Horiuchi et al[26]) have a high sensitivity to noise. The implemented observer works by making a cubic polynomial fit over a large number of measurements. The resulting cubic polynomial can be used to extrapolate positions, velocities, and accelerations forward in time. Fitting over many points provides a filtering effect (polynomial regression filtering[27]), addressing the noise and delay-compensation requirements simultaneously. The least-squares curve fit computation is efficient enough for real time use.

Because the observer feeds motions to both the actuator controller and the numerical simulation, 2 delay compensation levels are needed. The actuator delay level is based on estimates of the closed-loop latency. For passing kinematics to the numerical submodel, the time-step size and communication rate of the wind turbine simulation also need to be considered. In the present implementation, this amounts to an additional delay of 1 control loop period.

2.2.3 | Feedforward control and tension observer

The third control component provides a feedforward command so that force actuation is not limited by the bandwidth of the tension feedback controller. Knowing the cable stiffness, the cable tension can be changed rapidly and reliably using feedback from the servomotor encoders. A cable length rate of change command is calculated based on the desired thrust rate of change, $\dot{w}_d$:

$$\begin{aligned} \dot{l}_1 &= \frac{\dot{w}_d}{2K_{EA}}, \\ \dot{l}_2 &= -\frac{\dot{w}_d}{2K_{EA}}. \end{aligned} \tag{6}$$

Subject to the accuracy of the assumptions and actuator capabilities, this feedforward term will apply the desired dynamic thrust forces on the platform. The tension feedback controller is then reserved for the role of mean cable tension management and correcting any tension errors left over from the feedforward and motion accommodation control elements.

2.2.4 | Integrated controller

The 3 control components are integrated by summing their cable length rate of change commands. The result for each cable is then sent to the respective motor drive. Figure 3 shows the full hybrid coupling control system, including the abovementioned control elements for each cable as well as a tension observer to shield the low-bandwidth feedback controller from any rapid tension changes caused by the feedforward controller.

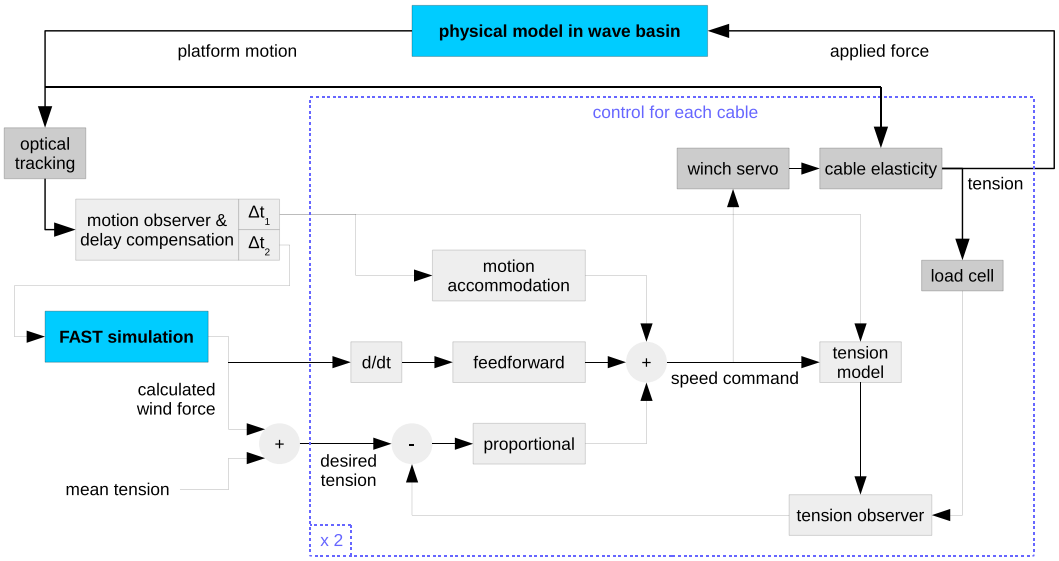

FIGURE 3 Final actuator control system including feedback, feedforward, and motion accommodation elements [Colour figure can be viewed at wileyonlinelibrary.com]

3 | HARDWARE IMPLEMENTATION AND TEST SETUP

The hybrid model coupling strategy was realized using the DeepCwind semisubmersible design and tested in 1:50-scale wave-basin experiments. The DeepCwind semisubmersible is a widely studied buoyancy-stabilized floating wind turbine design developed at the University of Maine and first tested in 2011 at MARIN.[28] At model scale, it features a 2.52-m diameter wind turbine meant to approximate the geometry and mass characteristics of the NREL 5 MW reference wind turbine design.[29]

3.1 | Physical submodel

The physical submodel used in the tests is the entire 1:50-scale DeepCwind semisubmersible prototype. Although aerodynamics are provided separately in the hybrid model, all of the structure's inertia is needed in the physical submodel.

The floating platform has 3 outer columns and a smaller fourth central column. The outer columns feature heave plates, and station-keeping is provided by 3 slack catenary chain moorings. The platform properties are given in Table 1 and are nearly identical to those of the original DeepCwind semisubmersible model[30] that was tested in 2011.

The turbine is the same as was used in the 2011 test campaign except that the nacelle mass is slightly reduced at 2.58 kg. Following the rotor geometry of the NREL 5 MW reference turbine,[29] it has a 126 m rotor diameter and a 90 m hub height at full scale. The 1:50-scale model turbine's performance is very different from the full-scale characteristics due to the Reynolds number scaling problems discussed earlier. To match the true-to scale thrust at rated wind speed, the blade pitch angles are set to 6.4° rather than 0°, and elevated wind speeds are used. The properties of the tested turbine are given in Table 2 and further details are available in Martin et al.[3] The instrumentation is unchanged from previous tests,[1] including rotor speed and torque measurements, a 3-axis accelerometer, and a 6-axis load cell at the tower top.

The testing environment is the University of Maine Alfond W^2 Ocean Engineering Laboratory. It features a 30 m long and 9 m wide wave basin with 4 m water depth. Sixteen force-controlled paddles create repeatable polychromatic sea states, and an elliptical beach minimizes wave reflection.

TABLE 1 DeepCwind semisubmersible platform properties

Draft	20 m
Airgap	10 m
Ballasted mass	13 444 000 kg
Displacement	13 987 m^3
Depth of CM	14.4 m
Roll inertia about CM	8.011E9 kg-m^2
Pitch inertia about CM	8.011E9 kg-m^2
Yaw inertia about CM	1.391E10 kg-m^2

Note. CM, center of mass.

TABLE 2 Properties of the DeepCwind wind turbine

Rotor diameter	126 m
Hub height above waterline	90 m
Overhang	10.58 m
Shaft tilt	0°
Precone	0°
Total tower-top mass	397 160 kg

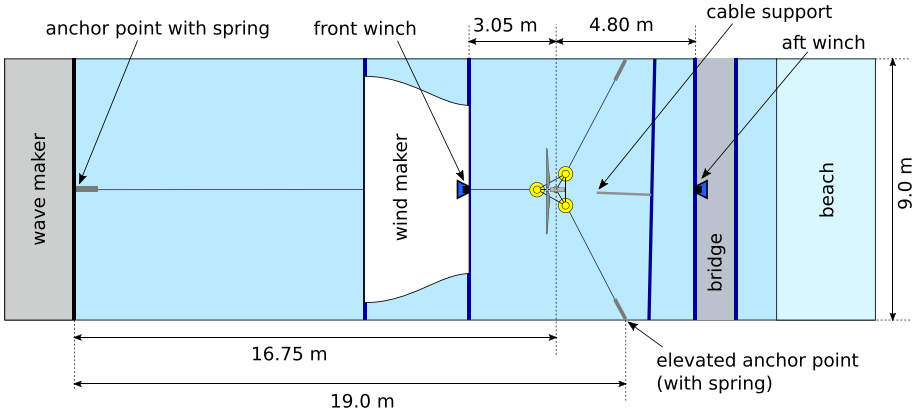

FIGURE 4 Layout of basin testing [Colour figure can be viewed at wileyonlinelibrary.com]

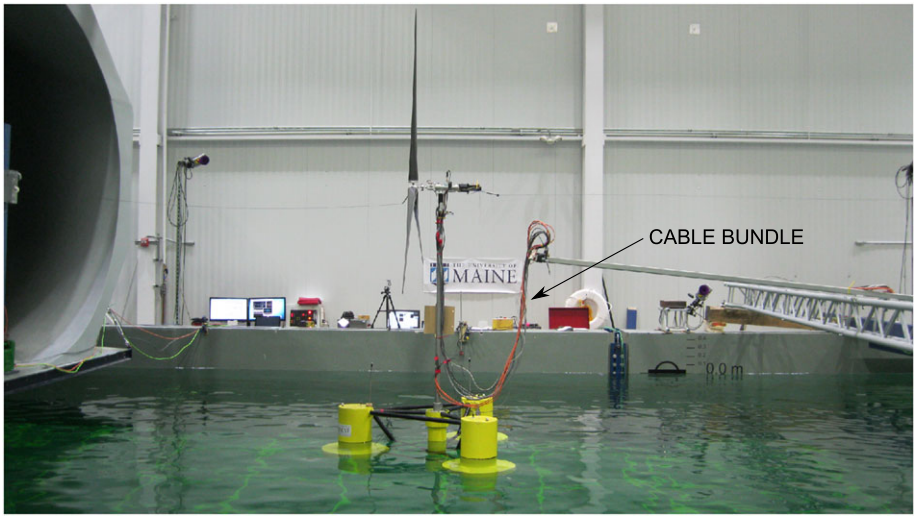

FIGURE 5 1:50-scale DeepCwind semisubmersible in basin with hybrid coupling attached [Colour figure can be viewed at wileyonlinelibrary.com]

Above the water, a wind generator 4.4 m wide and 3.2 m high can create steady winds of up to 7 m/s for use in conventional wind-wave tests. The wind generator consists of 4 rows of 8 fans, a series of screens, and a constriction to reduce turbulence. Figure 4 shows the testing layout.

To fit the 9 m width of the basin, the DeepCwind semisubmersible's 2 downwind mooring lines are truncated relative to the original 2011 tests. They are anchored at points 1.6 m above the basin floor (4 m water depth) through compliant springs to approximate the force-displacement characteristics of the untruncated mooring system.[31] The chain is of the same type as the 2011 tests.

A second difference in the support structure restoring properties relative to the 2011 tests is the heavier and less compliant cable bundle connected to the turbine tower, shown in Figure 5, which was observed to increase the surge restoring stiffness.

3.2 | Hybrid coupling system

The cable-based actuator hardware is comprised of 2 identical winch units, cables, and springs that connect the cables to the nacelle of the physical scale model. Each winch unit incorporates a speed-controlled servomotor, a load cell for tension measurement, and a pulley arrangement that

allows for a wide range of cable exit directions without affecting the tension measurement. Figure 6 shows the design. The servomotors are Teknic ClearPath model CPM-MCVC-2311S-RQN with 1280 count encoders, 4000 rpm rated speed and 0.41 N-m rated torque. These are connected without a gearbox to drums of 18.25 mm radius. These selections satisfy the torque, speed, and acceleration requirements calculated for testing of the DeepCwind semisubmersible design at 1:50 scale with a minimum safety factor of 2. Omega LPCW-7.5 planar-beam load cells provide tension measurement.

Because the feedforward controller requires a known overall cable stiffness and the feedback controller's disturbance rejection benefits from compliance in the cable system, springs are added between the cables and the nacelle. These give the cables a more linear overall stiffness behavior and allow for stiffness tuning to accommodate suitable tension levels for different model scales. Springs with 116 N/m stiffness were selected to suit the expected maximum thrust force of 7.9 N at model scale (982 kN full scale). A mean tension of 8 N allows a maximum applied force of 10 N while staying within the spring's linear range. The cables were composed of a high-strength upholstery thread with a measured unit-length stiffness of approximately $EA = 266$ N at the selected mean tension. The nacelle with the springs connected is shown in Figure 7. The forward spring was connected to the rotor hub, a distance of 212 mm ahead of the tower centerline. The aft spring was connected to the encoder at the aft end of the nacelle, a distance of 272 mm behind the tower centerline.

In the basin, the cable actuation system was set up over the existing conventional test setup. The 2 winch units were positioned at hub height along the center of the tank 3.05 m ahead and 4.80 m behind the undisplaced platform center position. Figure 1 shows the winch arrangement.

To prevent the long length from significantly reducing the cable stiffness, 4 strands of thread were run in parallel over most of the length, giving an approximate total stiffness of the thread running between each winch and spring of 380 N/m. With the 116 N/m spring stiffness in series, this gives a total stiffness of $k_{EA} = 90$ N/m.

The winch units are controlled by a National Instruments PXI real-time controller that centrally manages data acquisition and control operations for the hybrid coupling system and also runs the numerical submodel. A Qualisys Oqus optical tracking system with 3 infrared cameras takes position

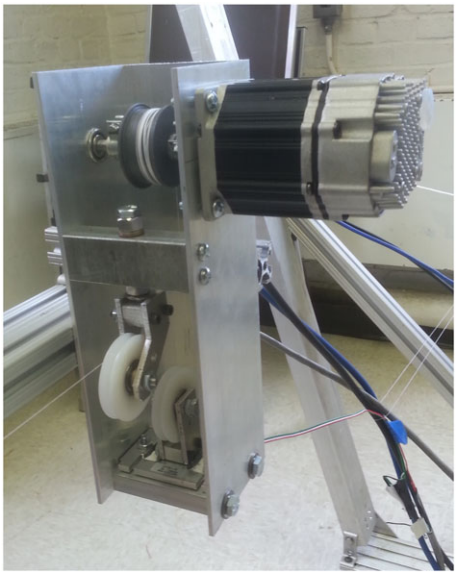

FIGURE 6 Winch unit design [Colour figure can be viewed at wileyonlinelibrary.com]

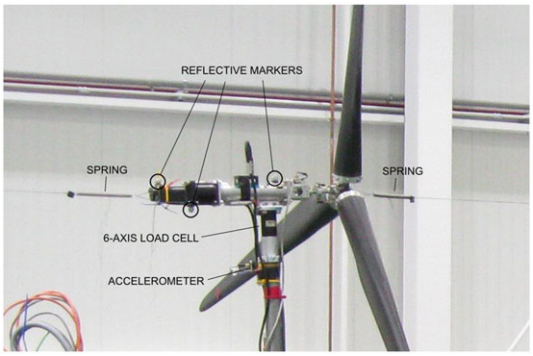

FIGURE 7 Turbine nacelle with cable system attached for hybrid model basin testing [Colour figure can be viewed at wileyonlinelibrary.com]

measurements at 100 Hz, which is the cycle rate of the cable control system. Five reflective markers on top of the platform and 3 on the nacelle (visible in Figure 7) enable 6-DOF position measurements of these bodies. The interconnected components of the coupling system are illustrated in Figure 8.

Extensive testing was done with the cable actuation system in isolation to test the control strategy, characterize the hardware performance, and tune the controller parameters. From a number of parameter studies, suitable system settings became clear. A load cell low-pass filter at 20 Hz provides a good balance of noise rejection and phase preservation. A delay compensation value of 20 ms improves the motion accommodation from the Qualisys motion-tracking measurements. Considering the 10 ms control loop period over which coupling with the numerical model occurs, the delay compensation in providing kinematics to the numerical model is increased to 30 ms. A tension feedback-control gain of 0.2 m/s/N provides the best gain characteristics at the important frequencies of 2 Hz and below, balancing stability with responsiveness under typical conditions.

3.3 | Numerical submodel

The numerical submodel used in the hybrid model tests was provided by FAST, a nonlinear time-domain floating wind turbine design code developed by the US NREL. Its aerodynamics module, AeroDyn, uses blade element momentum theory with tip- and hub-loss corrections as well as a Beddoes-Leishman dynamic stall model.[32] This simulation ability was used to calculate the aerodynamic forces on the wind turbine rotor, accounting for the rotor speed as well as the motions induced by the physical submodel movements. At each control system time step (every 10 ms), the optical measurement of nacelle position was processed, and the resulting motions used as input for the required number of FAST simulation time steps, from which the final wind turbine thrust force was taken and applied via differential cable tension onto the nacelle.

In the FAST simulation, the rotor was treated as rigid since the physical model rotor has a very high stiffness as a consequence of its material properties not being Froude scaled. Rotor mass was not included in the numerical submodel, since the full rotor structure is included in the physical submodel.

Two sets of wind turbine characteristics were simulated. The first set is matched to the experimental performance of the Froude-scaled model wind turbine and was developed previously at the University of Maine.[3,33] This allows direct comparison of the purely physical results and the hybrid model results. The second set of turbine characteristics is for the full-scale NREL 5 MW reference design, scaled down to the experiment while adjusting time so as to preserve Reynolds number. This represents the desired capability of testing a floating platform design in the basin with simulation-generated true-to-scale aerodynamic loads. It entails running a full-scale simulation at approximately 7 times real time, which is achievable using FAST with typical PC processing power when blade structural DOFs are disabled.

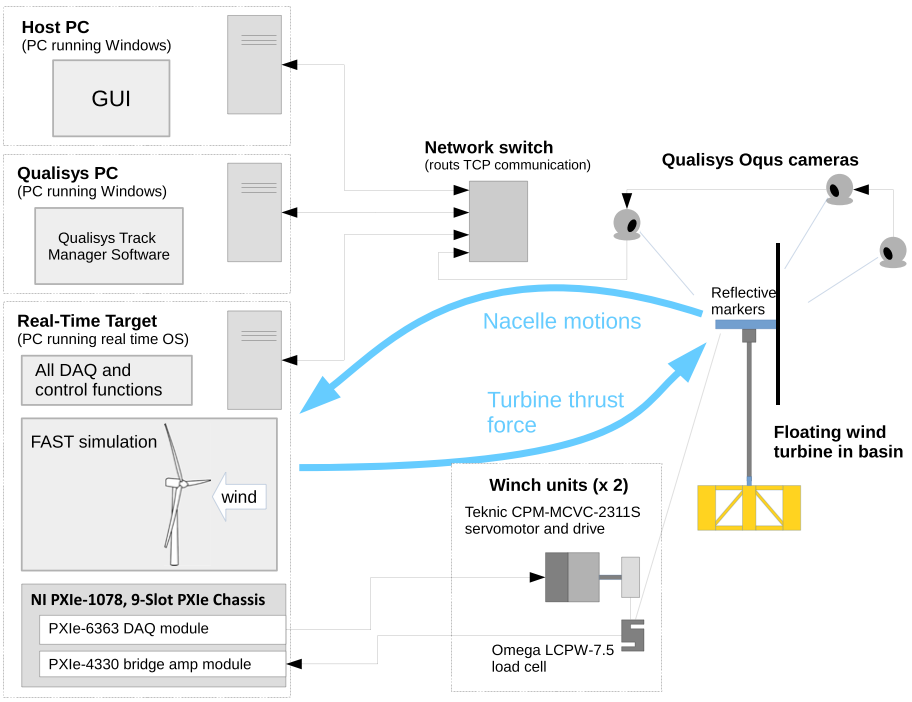

FIGURE 8 System electronics arrangement as used in basin testing. GUI, graphical user interface; DAQ, data acquisition; OS, operating system; TCP, transmission-control protocol [Colour figure can be viewed at wileyonlinelibrary.com]

4 | BASIN TESTING AND HYBRID COUPLING VALIDATION

The hybrid model of the DeepCwind semisubmersible was tested in between conventional wind-wave tests of the same load cases using the above-basin wind maker. The resulting consistency of conditions between conventional and hybrid model results presents a unique opportunity for validating the hybrid model behavior and exploring the effect of the capabilities only possible with the hybrid approach.

Seven test cases were considered for the purposes of this study, as listed in Table 3. Five involve the cable-based actuation system, each with a different scheme driving the applied force, from a simple zero-force command to a FAST/AeroDyn simulation of the turbine operating in turbulent wind. Two cases did not use the cable system and serve as a baseline for comparison. All data presented in this section are given at full scale, consistent with common practice for scale-model tests.

For comparability, the same sea state realization was used for all tests considered here. At full scale, the spectrum has a JONSWAP distribution with significant wave height of 7.1 m and peak spectral period of 12.1 seconds (full scale units). This is one of the sea states that was used in earlier tests of the DeepCwind tests at MARIN and is near what could be expected in the Gulf of Maine in 1-year storm conditions. As such, it is representative of floating wind turbine operating conditions that could be design driving.

All tests with an operating turbine used a rotor speed of 12.1 rpm. Simulations of the true-to-scale NREL 5 MW turbine used a blade pitch angle of 0° and a wind speed of 12 m/s, approximating the maximum-thrust operating conditions of the turbine. Tests or simulations with the Froude-scaled turbine used a blade pitch angle of 6.4° and a wind speed of 21 m/s. These are settings that were found necessary in previous experiments to compensate for the geometric Froude-scaled aerodynamics and achieve near the rated thrust force of the NREL 5 MW turbine.[34]

4.1 | Hybrid model validation

Validation is possible by running the same test cases with both the hybrid model and the conventional, purely physical model. The simplest analysis compares the wave-only response of the physical floating wind turbine model ("no wind - conventional") to the response of the same system when the cable actuation system is attached and set to provide zero net force on the platform ("no wind - hybrid"). This comparison without wind or turbine rotation evaluates the actuator's ability to be transparent to the physical system.

Figure 9 shows a sample of the measured net force applied by the cables during one of these tests. The root-mean-square amplitude of these undesired forces is 12.5 kN full scale (0.10 N model scale). This is approximately 1.5% of the maximum steady thrust force of the wind turbine and therefore an encouraging result. Figure 10 shows the power spectral density (PSD) of the same signal. Most of the energy can be seen to occur near 0.48 Hz, which is the natural frequency of the first tower bending mode.

Validation of the entire hybrid model involves comparing a conventional wind-wave test with a hybrid model test that uses FAST/AeroDyn to simulate the same aerodynamic scenario as was tested physically. For this purpose the turbine characteristics in the numerical model must match

TABLE 3 Summary of test cases used in the wind-wave basin

Test name	Wind	Modeled rotor	Aerodynamics model
no wind - conventional	0 m/s	DeepCwind	physical (no cables)
steady wind - conventional	21 m/s	DeepCwind	physical (no cables)
no wind - hybrid	none	none	cables: no net force
constant thrust - hybrid	none	none	cables: 800 kN force
steady wind - hybrid (basin model)	21 m/s	DeepCwind	cables: FAST/AeroDyn
steady wind - hybrid (NREL 5 MW)	12 m/s	NREL 5 MW	cables: FAST/AeroDyn
turbulent wind - hybrid (NREL 5 MW)	12 m/s turb.	NREL 5 MW	cables: FAST/AeroDyn

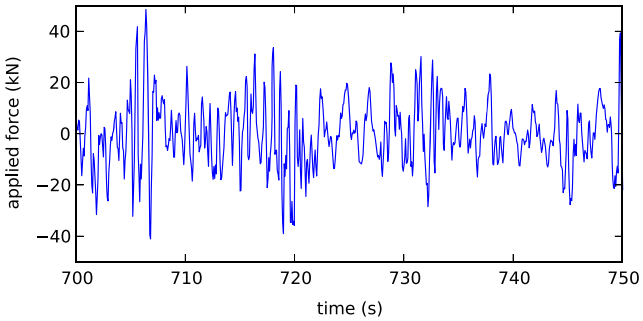

FIGURE 9 Applied force time series in zero-thrust test [Colour figure can be viewed at wileyonlinelibrary.com]

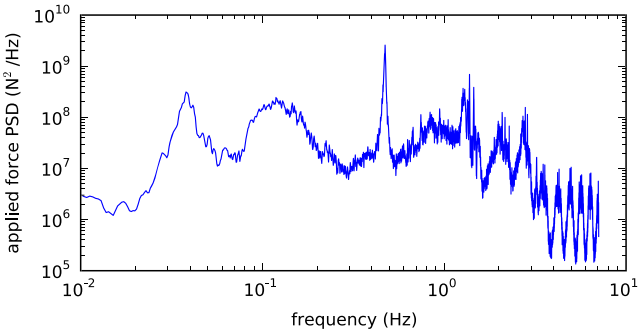

FIGURE 10 Applied force power spectral density (PSD) in zero-thrust test [Colour figure can be viewed at wileyonlinelibrary.com]

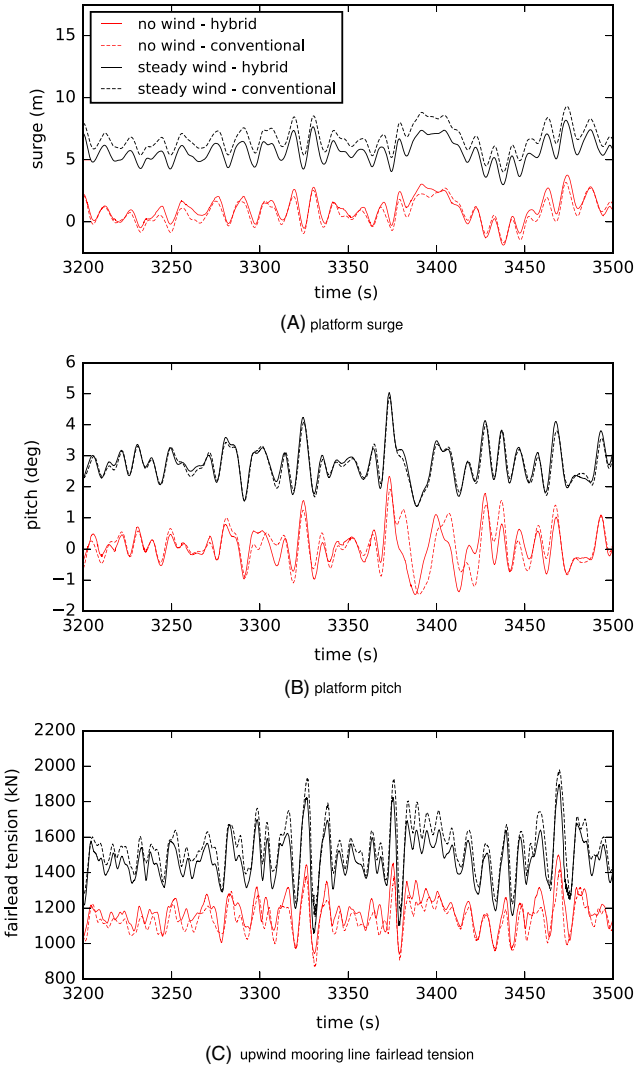

FIGURE 11 Comparison of hybrid (solid line) and conventional (dashed line) wave-only and wind-wave tests [Colour figure can be viewed at wileyonlinelibrary.com]

those of the physical scale-model turbine. This was done using the experimentally matched turbine properties referenced in section 3.3. The turbine operating parameters used in both physical and numerical models are 6.4° blade pitch, 12.1 rpm rotor speed, and 21 m/s wind speed (full-scale units).

Figure 11 compares time series of the system response in this case, as well as in the no-wind case described previously. Results from conventional (purely physical) model tests are shown with dashed lines and results from hybrid model tests are shown in solid. The general agreement between conventional and hybrid model approaches in each of these 2 cases reflects the successful performance of the hybrid coupling system: similar mean values reflect matching mean thrust forces, while similar amplitudes and phases indicate good matching of aerodynamic damping and proper mass

accounting with the numerical model. Meanwhile, differences between the wind and no-wind test cases are noticeable, with the presence of wind giving higher mean values of surge, pitch, and mooring tension as expected.

Table 4 compares the means and standard deviations measured from the same 3 response channels for the different tests. Hybrid and conventional test cases agree well. Comparing the no-wind cases, the largest difference is that the hybrid coupling system had a 9% reduction in the pitch standard deviation (the relative difference in mean surge is insignificant because the mean surge is almost zero). In the wind turbine–operating cases, the hybrid approach yielded somewhat lower mean surge and pitch values, likely a result of a lower mean thrust force arising from imperfect

TABLE 4 Comparison of hybrid and conventional approaches with and without wind

	Platform surge (m)		Platform pitch (°)		Upwind mooring ten (kN)	
	Mean	std	Mean	std	Mean	std
No wind – hybrid	0.920	1.118	0.08	0.66	1185	134
No wind – conventional	0.789	1.118	0.08	0.72	1140	127
% Difference	17%	0%	-1%	-9%	4%	6%
Steady wind – hybrid	5.734	1.099	2.76	0.64	1476	191
Steady wind – conventional	6.703	1.117	2.96	0.59	1539	202
% Difference	-14%	-2%	-7%	7%	-4%	-5%

Abbreviation: std, standard deviation.

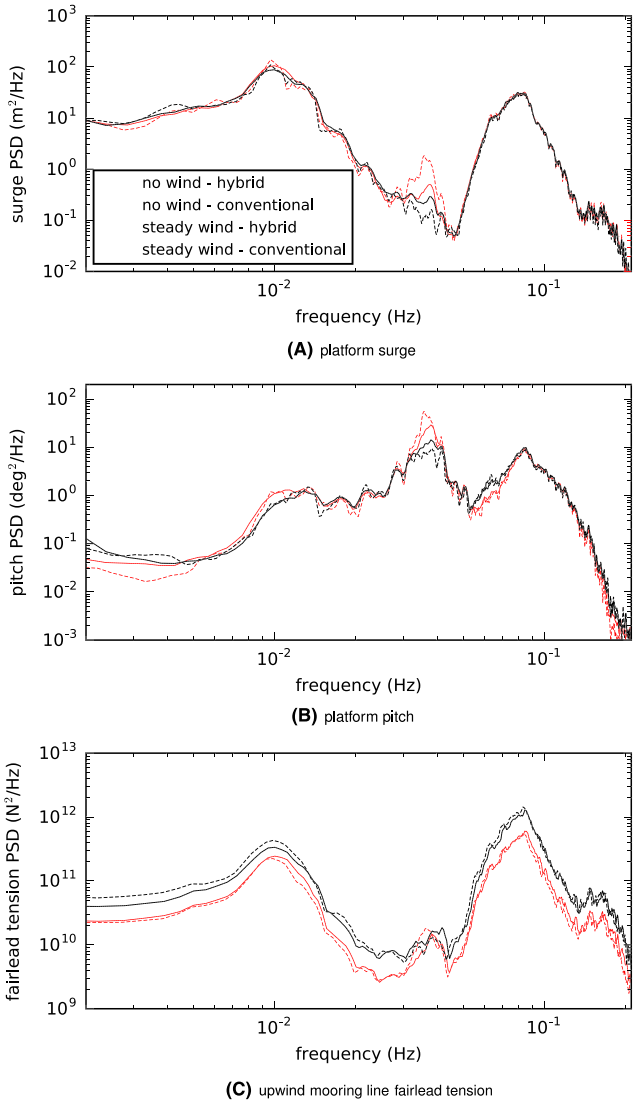

FIGURE 12 Power spectral density (PSD) comparison of hybrid (solid line) and conventional (dashed line) wave-only and wind-wave tests [Colour figure can be viewed at wileyonlinelibrary.com]

settings of the blade pitch angles and wind nozzle speed. This is something that could be corrected by tuning in a longer test campaign. The hybrid approach saw a 7% increase in pitch standard deviation, which may represent a limitation of the hybrid model implementation and warrants further investigation.

Figure 12 shows PSD plots of the same 3 channels. With or without wind, the hybrid model and conventional test PSDs can be seen to have good agreement over most of the spectrum. In surge, the agreement is especially good at the 0.01 Hz peak, corresponding to the surge natural frequency, and at 0.08 Hz, corresponding to the peak wave frequency. The greatest disagreement occurs around 0.035 Hz, the pitch natural frequency, suggesting that differences in pitch response are appearing in surge as a result of surge-pitch coupling.

In pitch, the height of the peak at 0.08 Hz, corresponding to the peak wave excitation, is similar across all cases. The cases with wind have slightly less excitation around the 0.035 Hz pitch natural frequency and the 0.01 Hz surge natural frequency, giving evidence that physical and numerical turbine aerodynamics both contribute damping on the fore-aft motions at hub height.

Differences in the fairlead tension PSD between hybrid and conventional tests are generally consistent with the differences in platform motion. The cases with wind have greater mooring tensions across the frequency range than the no-wind cases. This is a result of the nonlinear force-displacement relationship of the mooring; for a given sea state, an increase in mean surge will lead to increased tension fluctuations in the upwind mooring line.

Looking at Figure 12B, it appears that aerodynamic damping of pitch is greater in conventional tests than in hybrid tests. This is only obvious at the pitch natural frequency, where the pitch resonance allows such a subtle difference to be apparent. One explanation is that the cable-based actuator only applies forces longitudinally, neglecting the pitching moments and vertical force components that exist with the physical turbine. Another is that the spacing of the cable connections on the nacelle (0.48 m apart at model scale) could add a small spurious moment when the turbine is pitched.

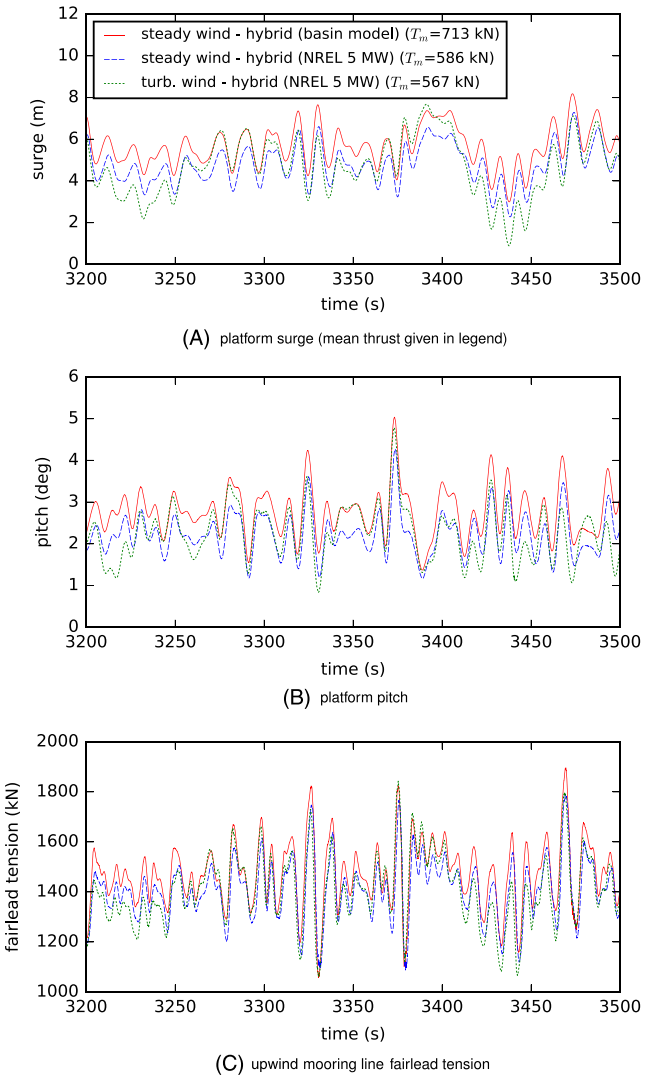

FIGURE 13 Sample time series of different hybrid model test cases. NREL, National Renewable Energy Laboratory [Colour figure can be viewed at wileyonlinelibrary.com]

Also likely, there could be differences between the numerical and physical wind turbine models. The numerical model was tuned for steady-state rather than dynamic characteristics,[33] and the ability of blade-element-momentum models to capture dynamics is limited.[35] Between these various factors, small differences in pitch response between hybrid and conventional tests are not surprising.

4.2 | Results with new hybrid model features

The main benefit of the hybrid approach is in replicating true-to-scale aerodynamics, which may not be possible with a physical approach. Toward that end, hybrid model tests were conducted with a numerical submodel of the NREL 5 MW reference turbine near its peak thrust condition in 12 m/s wind with the blade pitch angle set to 3.81° and the rotor speed set to 12.1 rpm. The first tests used steady wind. The next tests introduced a new capability that is difficult to achieve experimentally: prescribed wind turbulence. In this case the FAST/AeroDyn simulation used a stochastic wind field with 12 m/s mean speed and class B turbulence[36] (as defined by IEC 61400-1) calculated by TurbSim.[37] The sea state used earlier, a JONSWAP spectrum with 7.1 m significant wave height and 12.1 peak period, was retained in these tests.

Figure 13 shows time series excerpts from these 2 true-to-scale test cases as well as the test case described in the previous section that matches the experimental turbine performance. Similar fluctuations in the plotted channels across the 3 hybrid model test cases show that wave excitation is the dominant driver of these responses. The greatest deviations are apparent in the test case with wind turbulence, demonstrating the excitation

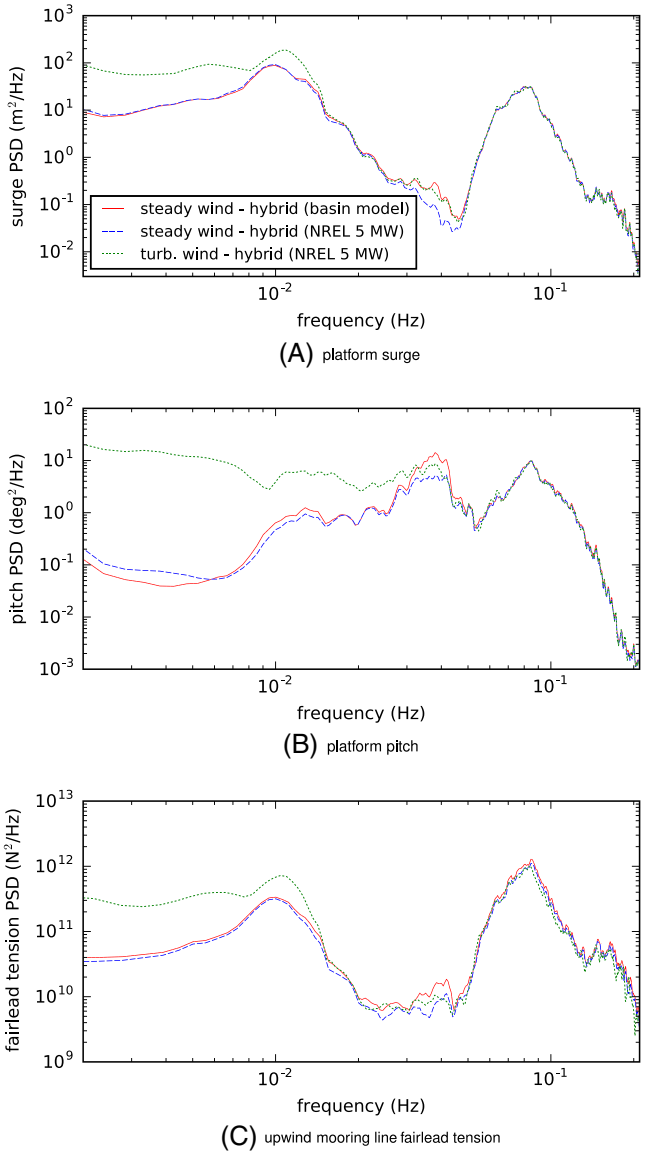

FIGURE 14 Power spectral density (PSD) comparison of different hybrid model test cases. NREL, National Renewable Energy Laboratory [Colour figure can be viewed at wileyonlinelibrary.com]

TABLE 5 Standard deviations of measured quantities in hybrid model testing

Turbine Sim.	Surge, (m RMS)	Pitch, (° RMS)	Upwind line tension, (kN RMS)	Downwind line tension, (kN RMS)
Constant thrust	1.11	0.69	196.5	40.1
Model turbine	1.10	0.64	191.4	41.2
NREL 5 MW	1.08	0.57	177.0	41.7
NREL turbulent	1.44	0.72	190.1	57.9

Abbreviations: RMS, root mean squared.

TABLE 6 Standard deviations of simulated quantities in hybrid model testing

Turbine Sim.	Tower-Top Mom., (kN-m RMS)	Rotor thrust, (kN RMS)	Nacelle acc., (m/s^2 RMS)	Blade-Root Mom., (kN-m RMS)
model turbine	223	20.9	1.90	351
NREL 5 MW	380	46.3	1.91	627
NREL turbulent	1482	118.9	2.04	1819

Abbreviations: RMS, root mean squared.

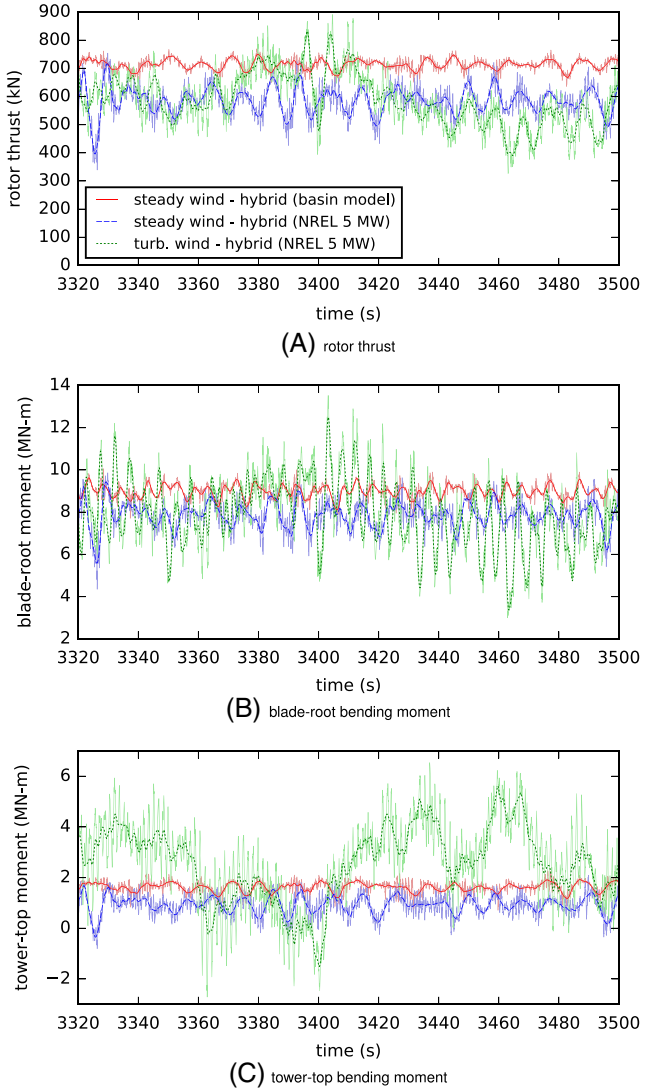

FIGURE 15 Sample FAST time series of different hybrid model test cases. NREL, National Renewable Energy Laboratory [Colour figure can be viewed at wileyonlinelibrary.com]

that unsteady wind introduces. The mean offsets of the different cases reflect the different mean thrust forces (denoted T_m in Figure 13A) between the 3 simulated turbine scenarios and are not reflective of any deficiency in the hybrid model approach.

Figure 14 shows PSDs of the same 3 channels. The peaks at 0.08 Hz correspond to the peak wave excitation and have very close agreement across the test cases, corroborating the synchronization visible in Figure 13. The peak in pitch response at the 0.035 Hz pitch natural frequency reveals interesting differences between the simulated conditions. The Froude-scaled model turbine case has the greatest pitch motion, indicating that it has the least aerodynamic damping. This can be understood by considering that the Froude-scaled wind turbine uses a wind speed of 21 m/s, almost double the 12 m/s wind speed used by the true-to-scale NREL 5 MW turbine. As such, the fluctuations in relative wind velocity induced by a given amount of pitch motion will be greater in a relative sense for a true-to-scale turbine than for the Froude-scaled turbine, translating into larger thrust force fluctuations and hence more aerodynamic damping and reduced pitch response. This is an expected and important difference made possible with the hybrid modeling approach.

When wind turbulence is added to the true-to-scale turbine scenario, the pitch excitation is increased at all frequencies up to and including the pitch natural frequency. As well, wind turbulence increases excitation in surge and mooring tension at the surge natural frequency and below. As evident in Figure 14, wind turbulence at class B levels has a significant effect on the floating wind turbine response. This speaks to the value of including wind turbulence in basin tests.

To provide a more quantitative comparison, Tables 5 and 6 show the standard deviations of important parameters measured from the basin and recorded from the simulation, respectively, in the 3 hybrid model test cases. These are given to show the differences in excitation between the

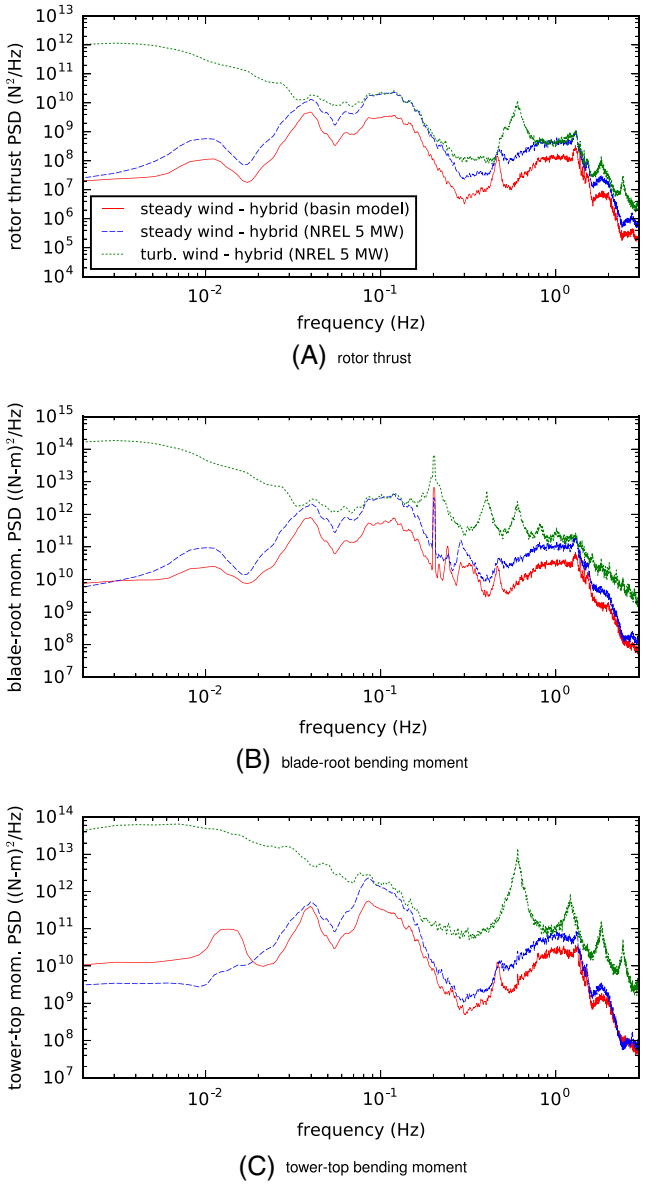

FIGURE 16 FAST PSD comparison of different hybrid model test cases [Colour figure can be viewed at wileyonlinelibrary.com]

conditions imposed on the simulation side: whether the simulated turbine is model scale or full scale and whether or not turbulence is included. Differences also exist in the mean values of these channels but are of little relevance to showing the capabilities offered by a hybrid model since mean forces and displacements can be easily adjusted by changing wind speed and rotor rpm. Table 5 shows the slightly reduced responses when simulating the true-to-scale NREL 5 MW turbine aerodynamics rather than the experimental turbine aerodynamics. In contrast, the constant-thrust case has much larger pitch motions since it excludes aerodynamic damping entirely. In the case with turbulent wind, the added excitation is apparent. Table 6 reveals changes in the standard deviations of loads and acceleration in the simulated turbine across the 3 different conditions. Using the true-to-scale NREL 5 MW turbine aerodynamics gives larger variances in all three loads, consistent with the already-discussed increase in aerodynamic damping relative to the Froude-scaled turbine aerodynamics. In the turbulent wind case, the further increase in relative wind velocity fluctuations causes a more than doubling of the rotor thrust and blade-root bending-moment standard deviations.

Figure 15 shows time series excerpts of rotor thrust, blade-root bending moment, and tower-top bending moment calculated by FAST in the 3 hybrid model tests. These channels contain a noticeable amount of excitation in the higher frequencies that are relevant for the wind turbine. The darker curves are the time series after filtering with a sixth-order Butterworth low-pass filter with 0.5 Hz cutoff frequency to show the lower-frequency signals that relate more directly to the platform motions. The rotor thrust fluctuations are visibly larger for the true-to-scale turbine than the Froude-scaled turbine, again reflecting the greater aerodynamic damping in the true-to-scale turbine. This translates into larger turbine structural loadings as are visible in the tower-top and the blade-root bending-moment plots. The presence of wind turbulence is seen to introduce significant low-frequency excitation in the loads.

Figure 16 shows PSDs of the same 3 channels. The excitation in the vicinity of 1 Hz reflects the high-frequency content seen in the time series of Figure 15 and likely represents optical motion tracking noise remaining in the motion observer output. As was visible in the time series plots, the true-to-scale turbine has generally larger load amplitudes than the Froude-scaled turbine. The presence of wind turbulence adds significant excitation at frequencies below the wave excitation but also at some higher frequencies. Significant blade-root and tower-top bending excitation at the 1P (0.2 Hz) and 3P (0.6 Hz) frequencies, respectively, reflect the spatial wind speed variations in the turbulent wind field.

5 | CONCLUSIONS

This study provides an experimental validation of a hybrid modeling approach to basin testing of floating wind turbines. A cable-based hybrid coupling system was developed, and a control strategy was designed to provide dynamic unidirectional forces on the turbine nacelle. Instrumented winch units were built and integrated with real-time control hardware and optical tracking equipment to complete the control loop. This system was then applied to a floating wind turbine basin test with the 1:50-scale DeepCwind semisubmersible.

Five tests run with the hybrid coupling system attached demonstrate a range of capabilities, from applying a steady thrust force or no force at all, to applying dynamic loads calculated in real time by a numerical wind turbine model. Two tests run without the cable-based actuator attached (one with the physical model turbine operating in response to the facility's wind generation capability) provide a baseline dataset representing the conventional testing approach. Using the same sea state realization in all tests allows time-series comparison.

Comparing the system response in wave-only conditions when the cable-based actuation system is attached and when it is disconnected shows good agreement, indicating that the cable-based system is successful at not interfering with the natural response. Hybrid model tests with the numerical submodel set to match the aerodynamic performance of the physical scaled wind turbine were compared with the matching purely physical wind-wave tests. The platform motions and mooring tensions in the conventional wind-wave test were matched very well by those of the hybrid model, validating the hybrid model approach.

Additional tests with the hybrid model featuring a true-to-scale wind turbine simulation and also including wind turbulence show the ability of the hybrid approach to provide features that are difficult to achieve with conventional methods. The significant difference in aerodynamic damping between Froude-scaled and true-to-scale wind turbine performance is clear in the results. Wind turbulence added a noticeable amount of excitation to the system. This demonstrates the value of a hybrid model approach for wave-basin testing in providing true-to-scale dynamic thrust loads and enabling other details such as realistic inflow turbulence—phenomena that are difficult to reproduce in purely physical wind-wave basin tests.

In summary, the results demonstrate experimentally that more realistic wind turbine performance can be represented with the hybrid model approach and that this has an important effect on basin-test results. It is also worth noting that, by handling wind loads with a numerical model, the hybrid model approach allows realistic floating wind turbine testing even in basin facilities that lack wind-generation capabilities.

ACKNOWLEDGEMENTS

The tests presented in this work were done with the generous help of Matthew Cameron, Raul Urbina, and Matthew Fowler at the University of Maine. Thanks goes to Velentin Chabaud, Giacomo Vissio, and Scott Beatty for discussions that were very helpful during the development of the hybrid coupling approach. Support from the Natural Sciences and Engineering Research Council of Canada is gratefully acknowledged.

ORCID

Matthew Hall http://orcid.org/0000-0002-0398-8320

REFERENCES

1. Martin H. Development of a scale model wind turbine for testing of offshore floating wind turbine systems. *MS Thesis*. Orono, Maine: University of Maine; 2011.
2. Müller K, Sandner F, Bredmose H, Azcona J, Manjock A, Pereira R. Improved tank test procedures for scaled floating offshore wind turbines. In: Proceedings of International Wind Engineering Conference - Support Structures & Electrical Systems; 2014; Hannover, Germany.
3. Martin HR, Viselli AM, Kimball RW, Goupee AJ. Methodology for wind/wave basin testing of floating offshore wind turbines. In: Proceedings of the 31st International Conference on Ocean, Offshore and Arctic Engineering; 2012; Rio de Janeiro, Brazil.
4. Fowler M, Kimball RW, Thomas DA, Goupee AJ. Design and testing of scale model wind turbines for use in wind/wave basin model tests of floating offshore wind turbines. In: Inproceedings of the 32nd International Conference on Ocean, Offshore and Arctic Engineering; 2013; Nantes, France.
5. de Ridder E, Otto W, Zondervan G, Huijs F, Vaz G. Development of a scaled down wind turbine for model testing floating wind turbines. In: Proceedings of the 33rd International Conference on Ocean, Offshore and Arctic Engineering; 2014; San Francisco, California.
6. Chabaud V, Steen S, Skjetne R. Real time hybrid testing of marine structures: challenges and strategies. In: Proceedings of the ASME 2013 32nd International Conference on Ocean, Offshore, and Arctic Engineering; 2013; Nantes, France.
7. Hall M, Moreno J, Thiagarajan K. Performance specifications for real-time hybrid testing of 1:50 scale floating wind turbine models. In: Proceedings of the ASME 2014 33rd International Conference on Ocean, Offshore and Arctic Engineering; 2014; San Francisco, California.
8. Azcona J, Bouchotrouch F, González M, et al. Aerodynamic thrust modelling in wave tank tests of offshore floating wind turbines using a ducted fan. *J Phys Conf Ser*. 2014;524(1).
9. Sebastian T, Lackner M. Characterization of the unsteady aerodynamics of offshore floating wind turbines. *Wind Energy*. 2013;16(3):339-352.
10. Jeon M, Lee S, Lee S. Unsteady aerodynamics of offshore floating wind turbines in platform pitching motion using vortex lattice method. *Renew Energy*. 2014;65:207-212.
11. Farrugia R, Sant T, Micallef D. A study on the aerodynamics of a floating wind turbine rotor. *Renew Energy*. 2016;86:770-784.
12. Bachynski EE, Chabaud V, Sauder T. Real-time hybrid model testing of floating wind turbines: sensitivity to limited actuation. *Energy Procedia*. 2015;80:2-12.
13. Jonkman JM, Buhl Jr. ML. FAST user's guide. Tech. Rep. NREL/EL-500-29798, Golden, Colorado, National Renewable Energy Laboratory; 2005.
14. Chabaud V. Real-Time hybrid model testing of floating wind turbines. *PhD Thesis*. Trondheim, Norway: NTNU; 2016.
15. Bachynski E, Thys M, Sauder T, Chabaud V, Saether L. Real-time hybrid model testing of a braceless semi-submersible wind turbine: part II: experimental results. In: Proceedings of the 35th International Conference on Ocean, Offshore and Arctic Engineering; 2016; Busan, South Korea.
16. Sauder T, Chabaud V, Thys M, Bachynski E, Saether L. Real-time hybrid model testing of a braceless semi-submersible wind turbine: part I: the hybrid approach. In: Proceedings of the 35th International Conference on Ocean, Offshore and Arctic Engineering; 2016; Busan, South Korea.
17. Kawamura S, Choe W, Tanaka S, Pandian SR. Development of an ultrahigh speed robot FALCON using wire drive system. In: Proceedings of 1995 IEEE International Conference on Robotics and Automation, 1995, Vol. 1; 1995; Nagoya. 215-220.
18. Surdilovic D, Bernhardt R. STRING-MAN: a new wire robot for gait rehabilitation. *Robotics and Automation*. 2004;5:2031-2036.
19. Verhoeven R. Analysis of the workspace of tendon-based stewart platforms. *PhD Thesis*: Universität Duisburg-Essen; 2004.
20. Alp A, Agrawal S. Cable suspended robots: design, planning and control. In: Proceedings of ICRA '02 IEEE International Conference on Robotics and Automation, 2002, Vol. 4; 2002; Washington, DC, USA. 4275-4280.
21. Roberts R, Graham T, Trumpower J. On the inverse kinematics and statics of cable-suspended robots. In: 1997 IEEE International Conference on Systems, Man, and Cybernetics, 1997. Computational Cybernetics and Simulation, Vol. 5; 1997; Orlando, FL, USA. 4291-4296.
22. Pott A, Bruckmann T, Mikelsons L. Closed-form force distribution for parallel wire robots. In: Proceedings of the 5th International Workshop on Computational Kinematics; 2009; Duisburg, Germany. 25-34.
23. Hall M. Hybrid modeling of floating wind turbines. *PhD Thesis*. Orono, Maine: University of Maine; 2016.
24. Zeng G, Hemami A. An overview of robot force control. *Robotica*. 1997;15(05):473-482.
25. Kalman RE. A new approach to linear filtering and prediction problems. *J Basic Eng*. 1960;82(1):35-45.
26. Horiuchi T, Inoue M, Konno T, Namita Y. Real-time hybrid experimental system with actuator delay compensation and its application to a piping system with energy absorber. *Earthquake Eng Struct Dynam*. 1999;28(10):1121-1141.
27. Proietti T, Luati A. Real time estimation in local polynomial regression, with application to trend-cycle analysis. *Ann Appl Stat*. 2008;2(4): 1523-1553.
28. Goupee A, Koo B, Lambrakos K, Kimball R. Model tests for three floating wind turbine concepts. In: Proceedings of Offshore Technology Conference (OTC 2012); 2012; Houston, Texas.
29. Jonkman JM, Butterfield S, Musial W, Scott G. Definition of a 5-MW reference wind turbine for offshore system development. Tech. Rep. 38060, Golden, Colorado, National Renewable Energy Laboratory; 2009.
30. Koo B, Goupee AJ, Kimball RW, Lambrakos KF. Model tests for a floating wind turbine on three different floaters. *J Offshore Mech Arct Eng*. 2014;136(2).
31. Fowler MJ, Goupee AJ, Viselli AM. Advances in model scale testing of floating offshore wind turbines utilizing the w2 Wind/Wave basin. In: Offshore Technology Conference; 2016; Houston, Texas.
32. Moriarty PJ, Hansen AC. AeroDyn theory manual. Tech. Rep., NREL; 2004.

33. Coulling AJ, Goupee AJ, Robertson AN, Jonkman JM, Dagher HJ. Validation of a FAST semi-submersible floating wind turbine numerical model with DeepCwind test data. *J Renew Sustain Energy*. 2013;5(2):023 116:1-29.
34. Goupee AJ, Koo B, Kimball RW, Lambrakos KF, Dagher HJ. Experimental comparison of three floating wind turbine concepts. *J Offshore Mech Arct Eng*. 2014;136(2).
35. Sebastian T, Lackner MA. A comparison of first-order aerodynamic analysis methods for floating wind turbines. In: Proceedings of the 48th AIAA Aerospace Sciences Meeting; 2010; Orlando, Florida.
36. Wind turbines - part 1: Design requirements. International Electrotechnical Commission, International Standard IEC 61400-1:2005(E); 2005.
37. Jonkman BJ, Kilcher L. TurbSim user's guide: Version 1.06.00. Tech. Rep, Golden, Colorado, National Renewable Energy Laboratory; 2012.

How to cite this article: Hall M, Goupee AJ. Validation of a hybrid modeling approach to floating wind turbine basin testing. *Wind Energy*. 2018;21:391–408. https://doi.org/10.1002/we.2168